Spatial evaluation of high-resolution modeled offshore winds using estimated winds derived from a network of HF radars

Greg Seroka, Josh Kohut, Laura Palamara, Scott Glenn, Hugh Roarty, Lou Bowers, Rich Dunk
Coastal Ocean Observation Laboratory
Rutgers University
New Brunswick, NJ USA
seroka@marine.rutgers.edu

***Abstract*—The temporal and spatial variability in the New Jersey offshore wind resource has large implications on the energy production for proposed offshore wind parks. The Rutgers University Weather Research and Forecasting (RU-WRF) mesoscale atmospheric modeling system can begin to diagnose as well as predict key sources of variability both in space and time, including sea and land breezes and frontal passages. While vertically validating model performance in coastal and offshore regions is readily achieved through the use of meteorological towers and approved remote sensing systems, horizontal evaluation of winds—especially at sufficiently high resolutions—can be difficult with pre-existing systems.**

We apply the high-resolution surface current mapping capabilities of a high frequency (HF) radar network to infer wind fields over the offshore domain of RU-WRF. Surface wind fields derived from the HF radar network are compared to 10m wind fields modeled by the RU-WRF; correlations are generally between 0.5 and 0.8 in the study domain.

Finally, to demonstrate the feature-tracking ability of the HF radar and RU-WRF model simulated offshore winds, we focus on a passing front and its associated thunderstorms. An area of divergence in RU-WRF modeled near-surface winds is evident as the thunderstorm line passes, likely caused by either a strong outflow boundary ahead of the thunderstorm front or directly from the cold downdraft in the core of the cold rain, which would reach the ocean's surface and diverge outwards. The forcing was so strong that the response was evident in both the HF radar currents and HF radar-inferred surface winds. The case warrants future analysis in surface ocean response to thunderstorm outflow boundaries and downdrafts, especially via the use of the HF radar-derived surface winds.

***Index Terms*—Offshore wind, atmospheric modeling, HF radar, CODAR, weather radar, WRF, air-sea interaction, coastal processes, complex correlation, coastal upwelling, surface ocean response**

I. Introduction

The temporal and spatial variability in the New Jersey offshore wind resource has large implications on the energy production for proposed offshore wind parks. The Rutgers University Weather Research and Forecasting (RU-WRF) mesoscale atmospheric modeling system can begin to diagnose as well as predict key sources of variability both in space and time, including sea and land breezes and frontal passages.

It is critical to evaluate the performance of RU-WRF not only in the vertical but also over the spatial horizontal study domain in order to identify areas for improvement and subsequently, if necessary, refine the model. Although vertical validation of winds can be performed with meteorological towers and approved remote sensing systems, horizontal spatial evaluation of winds, especially for offshore areas, can be difficult with pre-existing observational systems. Satellite-based scatterometers (e.g. QuikSCAT [1]) have historically provided wind measurements over the ocean. However, their relatively low spatial resolution of 25 km is not adequate for wind resource assessments associated with the spatial scale for most offshore wind turbine arrays. Furthermore, land contamination can occur within 25-37 km from the coast [2], precisely the development zone for non-floating offshore wind turbines.

II. Methods

We apply the high-resolution surface current mapping capabilities of a high frequency (HF) radar network (coastal radar, or CODAR) to infer wind fields over the offshore domain of the atmospheric model. The surface currents sampled by the shore-based CODAR system are forced by a combination of processes. In our study region the surface currents are largely driven by tides, buoyancy, and local winds [3,4]. The tides were extracted from the raw observed currents using standard least squares approaches [5]. We have found that in our region the relative importance of local winds in driving detided surface currents depends largely on stratification. During the winter season when the water column is mixed, bottom friction and pressure gradients drive the flow. During the summer, strong stratification isolates the slippery surface layer from the bottom leading to a surface current more dependent on the local wind forcing. Here we apply a regression model to estimate the offshore surface wind fields during this summer-stratified season at a resolution of 2 km across the designated study area.

We identified two sea breeze events during the summer-stratified season on which to focus our CODAR surface

current-based wind model: one without coastal upwelling (30 Aug-6 Sep 2012) and one with coastal upwelling (8-15 Sep 2012). We trained the model on one month of data spanning both events, 25 Aug to 25 Sep, while the water column was still stratified. We used measured wind from the Ocean City WeatherFlow site, which is on the coast centered on the study region and has good coverage over this time period. Wind observations were 75-minute center averaged to be consistent with the CODAR processing (Fig. 1).

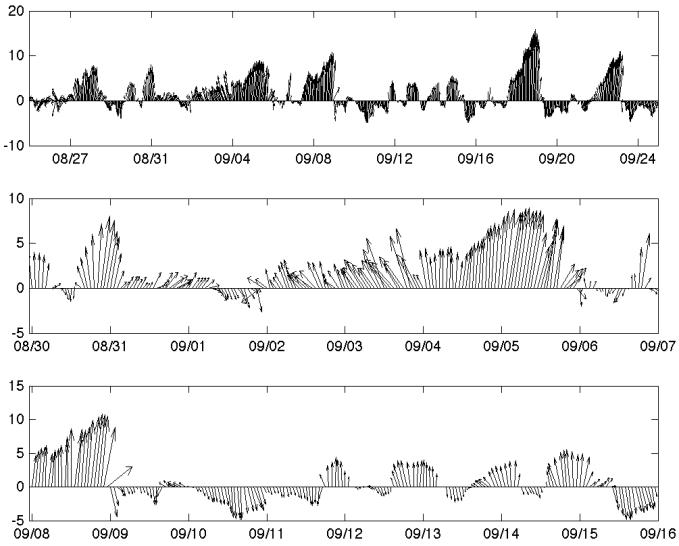

Fig. 1: Hourly 75-minute averaged wind measurements at the Ocean City WeatherFlow site for the time period used to train the surface current-based wind model. Top panel shows winds for the entire time period, middle panel shows the early September 2012 sea breeze case, and the bottom panel shows the mid-September 2012 sea breeze case. Tick marks are at 00:00 GMT for day noted.

The wind model is based on the correlation between the local wind observation in Ocean City, NJ and the surface current observations at each grid point in the survey region [5]. For each grid point we calculated the complex correlation between the local wind observation and the observed detided surface current. The magnitude across the field had a mean of 0.56 and a maximum of 0.73, and most of the region had a correlation higher than 0.4. The phase indicates that the highest correlated current was shifted to the right of the wind with an angle that ranged from about 0 to 60° across the field. These values are based on a zero time lag between the wind and current. Three points in regions of high correlation were used to determine the time lag that yielded the highest correlation between surface winds and currents. For each of these points we lagged the currents by 0 to 12 hours and recalculated the complex correlation. For each point, the highest correlation between wind and current peaked with a lag of about three hours. This indicates that the surface currents lag the wind forcing by approximately three hours (Fig. 2).

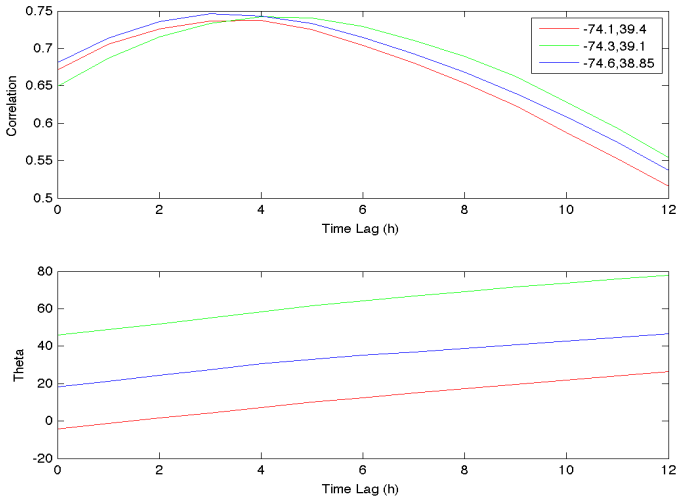

Fig. 2: Time-lag dependent complex correlation magnitude (top) and angle offset between highest correlated components of wind and surface current (bottom) for three points in regions of high correlation (red: northernmost, green: central, blue: southernmost). The correlation peaks at a time lag of around three hours, and offset angle steadily increases with increasing time lag.

The complex correlation was then recalculated with this lag across all grid points. The majority of the study region had a resulting a mean correlation of 0.62 and a maximum of 0.92, with over 50% of the region at a correlation above 0.6. The new correlation values increased with lowest values near the edges and the highest values again near the center of the CODAR coverage (Fig. 3). Surface currents were rotated based on the angles shown in the right panel of Fig. 3 and a best-fit line applied to the rotated surface u (v) current and measured u (v) wind three hours previous as in [5]. Estimated wind maps were then generated by rotating CODAR-measured surface currents and applying the best-fit equations to the rotated currents. The resulting surface current-based wind estimates were the basis for the spatial evaluation of the offshore wind fields predicted by the RU-WRF model. An example of the final suite of imagery that was used to spatially evaluate RU-WRF offshore winds is presented in Fig. 4, which includes CODAR detided currents, surface winds, and RU-WRF modeled 10m winds.

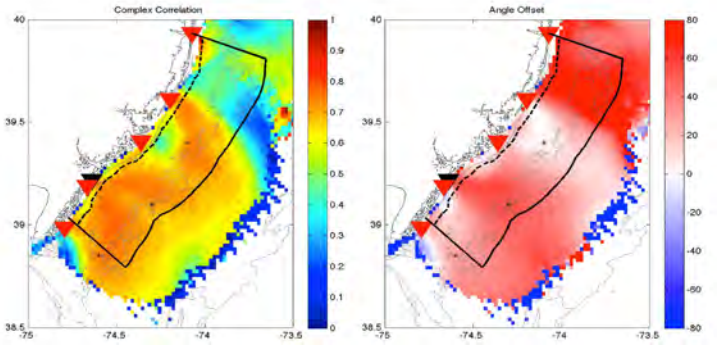

Fig. 3: Magnitude of complex correlation and angle offset between the highest correlated components of the wind and surface currents with a three-hour lag. Black triangle: location of the Ocean City WeatherFlow site, red triangles: 13 MHz CODAR sites, solid line: study area offshore wind (extending 20 nm offshore), dashed line: boundary between federal and state waters (3 nm offshore), asterisks: test locations for time lags shown in Fig. 2.

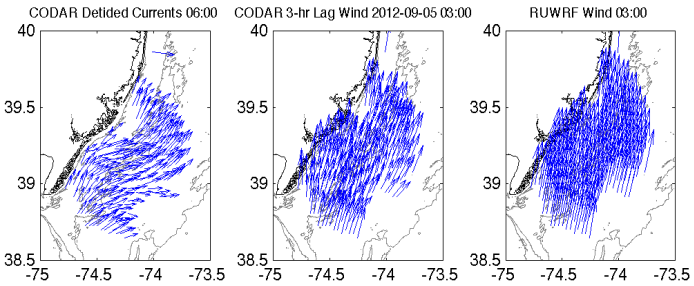

Fig. 4: Detided surface currents on 5 Sep 2012, 06:00 GMT (left), wind predicted for 03:00 based on those currents (center), and RU-WRF model 10m wind at 03:00 (right).

Because our surface wind estimates are derived directly from CODAR currents, any uncertainty in the current measurements would produce a subsequent uncertainty in the wind estimates. Several prior studies [6,7] using acoustic Doppler current profilers (ADCPs) to evaluate HF radar currents measurements found the intrinsic 5 MHz HF radar radial uncertainty to be of O(5 cm/s). We can assume an uncertainty of the same order or smaller for this study which uses the shorter range, higher-resolution measurements from a 13 MHz HF radar system. Accounting for this surface current uncertainty in our wind model produces O(0.75 to 1 m/s) uncertainty in our estimated winds.

III. Results

For the upwelling and non-upwelling case studies, we used the CODAR surface wind estimate to evaluate RU-WRF performance offshore throughout the study region. In this evaluation, we limited the comparison to those grid points in which the correlation between the CODAR currents and Ocean City WeatherFlow winds was at least 0.6. For these grid points, the comparison between CODAR winds and RU-WRF model winds were determined for the upwelling and non-upwelling cases. For the non-upwelling case between 30 Aug 2012 and 6 Sep 2012, the correlation coefficient was at least 0.5 across the study region, with a large area of 0.65 correlation near the center of the field. Angle offset values were consistently between 0° and about 20° across the study region indicating that the most correlated RU-WRF model wind vector is shifted to the right of the CODAR wind estimate (Fig. 5).

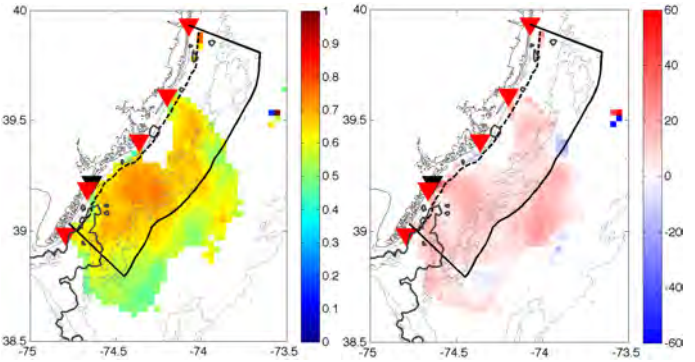

Fig. 5: Magnitude of complex correlation (left) and angle offset (right) between the CODAR-predicted surface wind (e.g. Fig. 4, center) and RUWRF modeled 10m wind (e.g. Fig. 4, right), for the non-upwelling case (30 Aug 2012-6 Sep 2012). Black triangle: location of the Ocean City WeatherFlow site, red triangles: 13 MHz CODAR sites, black solid line: study area coinciding with the study area for offshore wind (extending 20 nm offshore), dashed line: boundary between federal and state waters (3 nm offshore), dark gray solid contour: 24°C isotherm of SST, showing minimal to no coastal upwelling occurring in the study area.

The upwelling case, between 8 Sep 2012 and 15 Sep 2012, had a different spatial pattern in the comparison between CODAR wind estimates and RU-WRF model simulated offshore winds. For the upwelling case, there was a cross and along-shelf gradient in the correlation with the lowest values very near shore close to the center of the field. Farther offshore there is a faint banding pattern with the highest correlations centered on the middle of the field (Fig. 6). The region of low correlation near shore with values less than about 0.6, coincides with the core of coastal upwelling that occurred for much of the time period. This zone of upwelling is depicted by the gray contour of 22°C SST along the coast of Atlantic City. Inside the upwelling center the water column is well mixed [8]. Under these mixed conditions it has been shown the CODAR surface currents are less responsive to local winds. Therefore, the low correlation in this upwelling center is likely more a result of uncertain CODAR estimates of the winds rather than inaccuracies in the RU-WRF model winds.

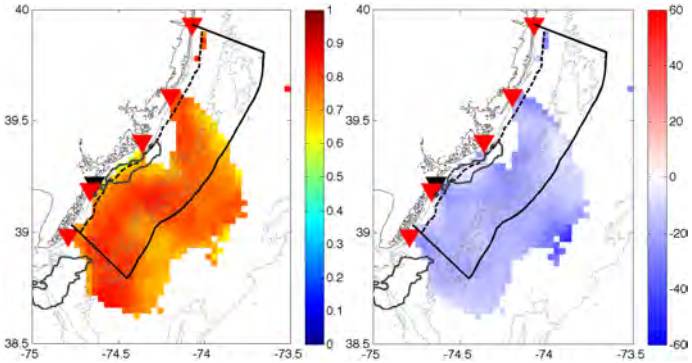

Fig. 6: Magnitude of complex correlation (left) and angle offset (right) between the CODAR-predicted surface wind and RUWRF modeled 10m wind, for the upwelling case. Black triangle: location of the Ocean City WeatherFlow site; Red triangles: 13 MHz CODAR sites; Black solid line: study area; Dashed line: boundary between federal and state waters: Gray solid contour: 22°C isotherm of SST, showing coastal upwelling.

The faint bands of lower correlation in the alongshore direction farther offshore are spaced approximately 30 km apart, matching the scale of the inshore upwelling center. It has been shown that these upwelling centers are characterized by an alongshore velocity jet running up the NJ coast along the offshore edge of the surface front [8]. A closer examination of the surface currents over this upwelling case show that the surface currents offshore tend to follow the shape of the upwelling center with a general flow along the coast near the southern boundary of our survey region that turns sharply offshore just south of the upwelling center before turning alongshore farther north. This spatially dependent perturbation in the flow around the upwelling center could bias the wind estimates from the CODAR systems. Furthermore, the banding that is evident over the upwelling

case could also be in part due to the geometry of the CODAR sites.

CODAR derived wind field estimates were used to evaluate the RU-WRF model performance in resolving the spatial structure of the offshore wind field. Wind estimates derived from CODAR data appear to be influenced by the near-shore upwelling center, and perhaps the geometry of the CODAR sites during the upwelling case. Therefore, we chose to concentrate this analysis on the non-upwelling case. During the non-upwelling case the CODAR estimated winds were more uniformly correlated with the RU-WRF model results over most of the study region.

Fig. 7 depicts a subtle banding in convergence/divergence west to east in the RU-WRF modeled winds (Fig. 7, right) as well as the CODAR-derived surface wind field (Fig. 7, center) on 4 Sep 2012 at 19:00 GMT. A convergence band is evident on the southwestern edge of the study area in both the CODAR wind and RU-WRF wind fields. Just to the east, an area of lighter, more divergent winds is evident in both fields, and then farther east another area of higher, more convergent winds. In general, there is good overall correlation between wind direction in both the CODAR product and RU-WRF model (i.e. both from the south), while CODAR de-tided currents are more variable from the southwest, west, and south at that time as one moves north up the coast (Fig. 7, left).

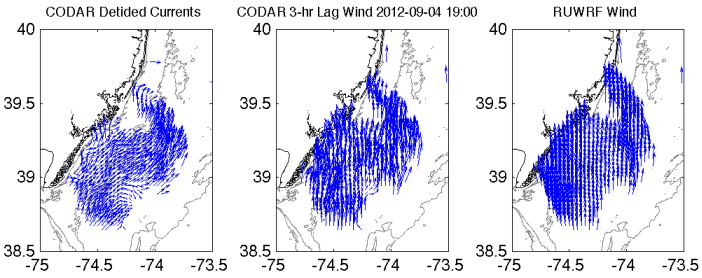

Fig. 7: Detided surface currents on 4 Sep 2012, 19:00 GMT (left), wind predicted for 19:00 based on the currents 3-hrs earlier (center), and RU-WRF modeled 10m wind at 19:00 (right).

Throughout the model study the RU-WRF model winds showed significant spatial variability associated with local processes including fronts associated with the sea breeze and passing thunderstorms. To demonstrate the feature tracking of the CODAR and RU-WRF model simulated offshore winds, we focused on a passing front between about 18:00 GMT on 5 Sep 2012 and 06:00 GMT on 6 Sep 2012. A strong line of thunderstorms developed along the front; at 23:00 GMT, the line of storms was directly over the northern section of the study area. At the same time, the near-surface wind response to the thunderstorms was evident in our RU-WRF model run with a distinct area of surface divergence located in the northeastern section of the study area, offshore of Tuckerton, NJ (Fig. 8, bottom left).

The surface divergence in the winds was likely caused by either a strong outflow boundary ahead of the thunderstorm front or directly from the cold downdraft in the core of the cold rain, which would reach the ocean's surface and diverge outwards. The forcing was so strong that the response was evident in both the CODAR detided ocean currents (Fig. 8, top left) that are directed offshore in the coincident area, and the CODAR-derived surface winds (Fig. 8, top right) that are directed outward from the thunderstorm core and offshore of Tuckerton. A time-series further indicates the slow progression of the thunderstorm line, and along with it the southeastward movement of the surface divergence in the winds as well as currents.

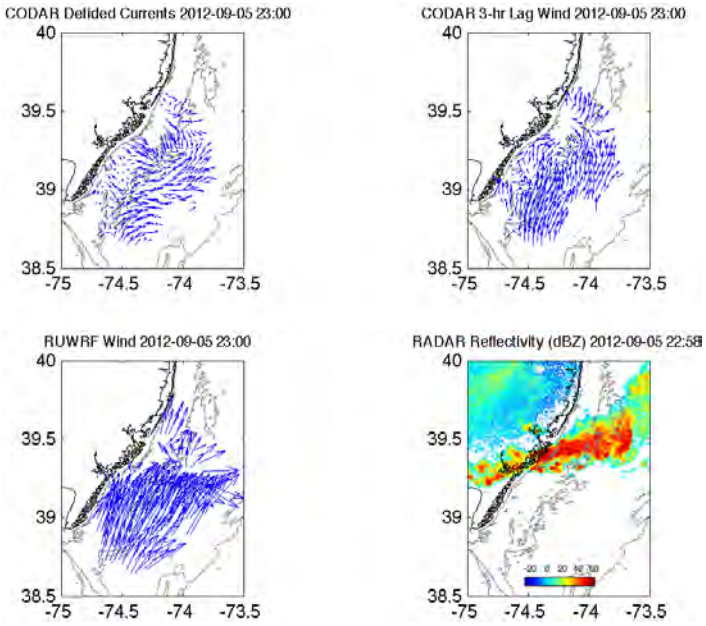

Fig. 8: Detided surface currents on 5 Sep 2012 23:00 GMT (top left), wind predicted for 23:00 GMT based on the currents 3 hrs earlier (top right), RU-WRF model 10m wind at 23:00 (bottom left), and weather radar reflectivity depicting a line of strong thunderstorms at 22:58 GMT (bottom right).

IV. Conclusions

A method for estimating surface winds using a network of HF radars has been developed, and the resulting wind estimates were used to spatially evaluate the performance of a high-resolution atmospheric model in the coastal regime. When pairing this spatial evaluation (i.e. in the xy-plane across time) with vertical validation (i.e. in the z direction, across time) we can begin to determine the accuracy of the model's depiction of mesoscale atmospheric processes in all four dimensions (i.e. in the x,y, and z directions across time).

The thunderstorm case study presented above provided a period of time that showed excellent correlation between modeled surface wind divergence and observed ocean response, possibly due to the slow-moving nature of the cold front. Because maximum correlation between currents and winds occurred at a three-hour lag, any phenomenon that has a lifetime in the study domain shorter than three hours may not be effectively captured. The case warrants future analysis in surface ocean response to thunderstorm outflow boundaries and downdrafts, especially via the use of the CODAR-derived surface winds. In addition, the methods developed above can be used to spatially evaluate the model's performance during sea/land breeze events, which potentially have a significant

impact on the daily timing of offshore wind power production during the summer peak energy demand season.

ACKNOWLEDGMENTS

This work was funded by a grant from the New Jersey Board of Public Utilities: "An Advanced Atmospheric/Ocean Assessment Program Designed to Reduce the Risks Associated with Offshore Wind Energy Development Defined by the NJ Energy Master Plan and the NJ Offshore Wind Energy Economic Development Act".

REFERENCES

[1] Shirtliffe, G. M. (1999), QuikSCAT science data product user's manual, overview, and geophysical data products. Version 1.0. JPL D-18053, Jet Propulsion Laboratory, Pasadena, CA, 90 pp.

[2] Chao, Y., Z. Li, J. Kindle, J. Paduan, and F. Chavez (2003), A high-resolution surface vector wind product for coastal oceans: Blending satellite scatterometer measurements with regional mesoscale atmospheric model simulations, Geophys. Res. Lett., 30(1), 1013, doi:10.1029/2002GL015729.

[3] Beardsley, R. C., W. C. Boicourt, and D. V. Hansen (1976), Physical oceanography of the Middle Atlantic Bight, Limnol. Oceanogr. Spec. Symp., 2, 20 – 34.

[4] Beardsley, R. C., and D. B. Haidvogel (1981), Model studies of wind driven transient circulation in the Middle Atlantic Bight, part 1: Adiabatic boundary conditions, J. Phys. Oceanogr., 11, 355 – 375.

[5] Kohut, J. T., S. M. Glenn, and R. J. Chant (2004), Seasonal current variability on the New Jersey inner shelf, J. Geophys. Res., 109, C07S07, doi:10.1029/2003JC001963.

[6] Kohut, J., H. Roarty, and S. M. Glenn (2006), Characterizing observed environmental variability with HF Doppler radar surface current mappers and acoustic Doppler current profilers: Environmental variability in the coastal ocean, IEEE J. Oceanic Eng., 31, 876 – 884, doi:10.1109/ JOE.2006.886095.

[7] Chapman, R. D., and H. C. Graber (1997), Validation of HF radar measurements, Oceanography, 10, 76 – 79.

[8] Chant, R. J., S. M. Glenn, J. Kohut (2004), Flow reversals during upwelling conditions on the New Jersey inner shelf, J. Geophys. Res., Vol. 109, No. C12, C12S03. 10.1029/ 2003JC001941.